Proc. NIPR Symp. Polar Meteorol. Glaciol., **10**, 127–137, 1996

CLASSIFICATION OF POLAR SATELLITE DATA USING IMAGE FEATURES AND DECISION TREE CLASSIFIER

Ken'ichiro MURAMOTO[1] and Takashi YAMANOUCHI[2]

[1]*Department of Electrical and Computer Engineering, Faculty of Engineering, Kanazawa University, 40–20, Kodatsuno 2-chome, Kanazawa 920*
[2]*National Institute of Polar Research, 9–10, Kaga 1-chome, Itabashi-ku, Tokyo 173*

Abstract: In the polar region, it is difficult to discriminate between clouds and ground surface from satellite visible or infrared data, because of the high albedo and low surface temperature of snow and ice cover. In this paper, a method to classify clouds, sea ice and ground is proposed. This study is based upon analysis of the NOAA/AVHRR infrared images in Antarctica. The algorithm consists of two major approaches: estimating image features and a classification algorithm. A decision tree classifier is designed to classify the region into one of three classes using six image features. Though sea ice and ground can be largely separated using only one feature, more than three features are necessary to separate clouds.

1. Introduction

Antarctic sea ice is one of the important factors that affect the polar climate and the global atmospheric system (GORDON and TAYLOR, 1975; MAYKUT and UNTERSTEINER, 1971; ROBOCK, 1983). Clouds in the Antarctic are also important because of their strong radiative influence on the energy balance of the snow and ice surface (SALTZMAN and MORITZ, 1980). Remote sensing observation from a meteorological satellite offers the best available means to understand polar surface conditions, because of their homogeneity over a wide area.

However, in the polar region, cloud, snow and ice have almost the same albedo in the visible channel and the same brightness temperature in the infrared channel. Therefore, it is difficult to distinguish among these regions using only the threshold of gray level of a satellite image (COAKLEY and BRETHERTON, 1982; DESBOIS *et al.*, 1982). YAMANOUCHI and KAWAGUCHI (1992) show that a method to detect clouds by the brightness temperature difference of two channels is thoroughly effective in the sunlight season, but not perfect in all seasons and at all times.

In this paper, techniques for classifying Antarctic satellite images into clouds, sea ice and ground using single channel data are proposed. The approaches can be divided into the following four steps: (1) Representative areas of clouds, sea ice and ground were selected subjectively. (2) Six types of features were computed in each selected area. (3) A decision tree classifier was designed to classify the region into one of three classes using the features. (4) Features of the whole area were calculated and classified using the decision tree classifier. Infrared channel data were used for developing a complete classifying method that will be effective in all seasons and at all times.

2. Data

AVHRR data received from the NOAA satellite have been processed primarily and stored at Syowa Station, Antarctica, since 1987 (YAMANOUCHI *et al.*, 1991). We obtained the image data of the area near Syowa Station from the National Institute of Polar Research. The area is composed of 512×512 pixels with spatial resolution 2.2 km. At each pixel location, the image brightness was quantified into 256 gray levels for computer graphics display.

3. Calculation of Features

3.1. Subregion

The satellite image area was divided into square areas. Features at each location (x, y) of the subregion were obtained from a (32×32)-pixel block area in a sample image as shown in Fig. 1. The subregion was moved to the next pixel location in the image and the calculation was repeated. This continued until all pixel locations were covered.

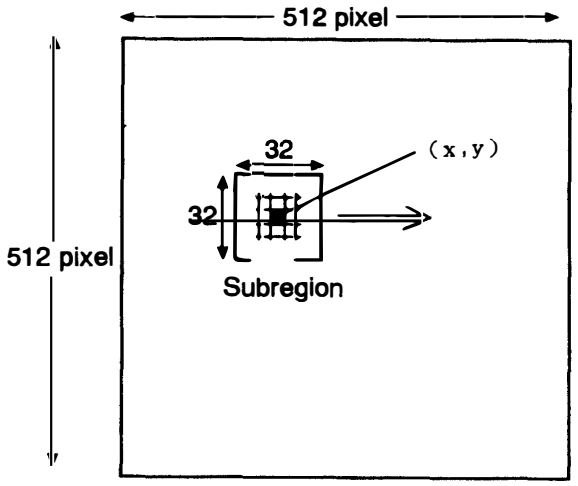

Fig. 1. Square subregion area in sample image centered at (x, y).

3.2. Average and standard deviation of the brightness temperature of each pixel in a subregion

Averaging of the brightness temperatures of the pixels is one of the most effective approaches to image segmentation, because usually a uniquely separated area is larger than any other feature. If each average value of subregions is grouped into two classes, the area may be classified into two regions. However, large parts of area are not classified in many cases. The standard deviation provides one measure of the variability, this value is much easier to compute than the fractal and texture.

3.3. Fractal dimension

Many natural surfaces look qualitatively the same at different scales. This self-similar property means that extra detail appears at quantitatively the same rate over many

changes in scale or magnification. The fractal dimension gives a quantitative property of a surface (MANDELBROT *et al.*, 1984). The gray level function in the region is defined by brightness temperature. The method relies on the assumption that regions of an image having a particular structure will usually produce a fractal gray level surface, with a particular value of the fractal dimension. It is difficult, however, to measure a fractal dimension strictly according to the definition.

For convenience, we used a three-dimensional cube to measure the fractal surface's dimension by covering the surface with a minimal number of cubes. As shown in Fig. 2a, a three-dimensional cube of edge r was used to measured the fractal dimension D by covering the image intensity surface cubes. If the total number of cubes which cover this surface is proportionally increased with decreasing scale r, then the fractal dimension related to the surface roughness of the brightness temperature can be obtained. This dimension can be obtained by plotting, on a log-log scale, the total number of cubes for edge r against the length of edge r. The resulting plot has slope $-D$ as shown Fig. 2b. If a surface is a perfect fractal surface, then the fractal dimension will remain constant over all ranges of edge r. Generally, there are scale range limitations of fractal dimen-

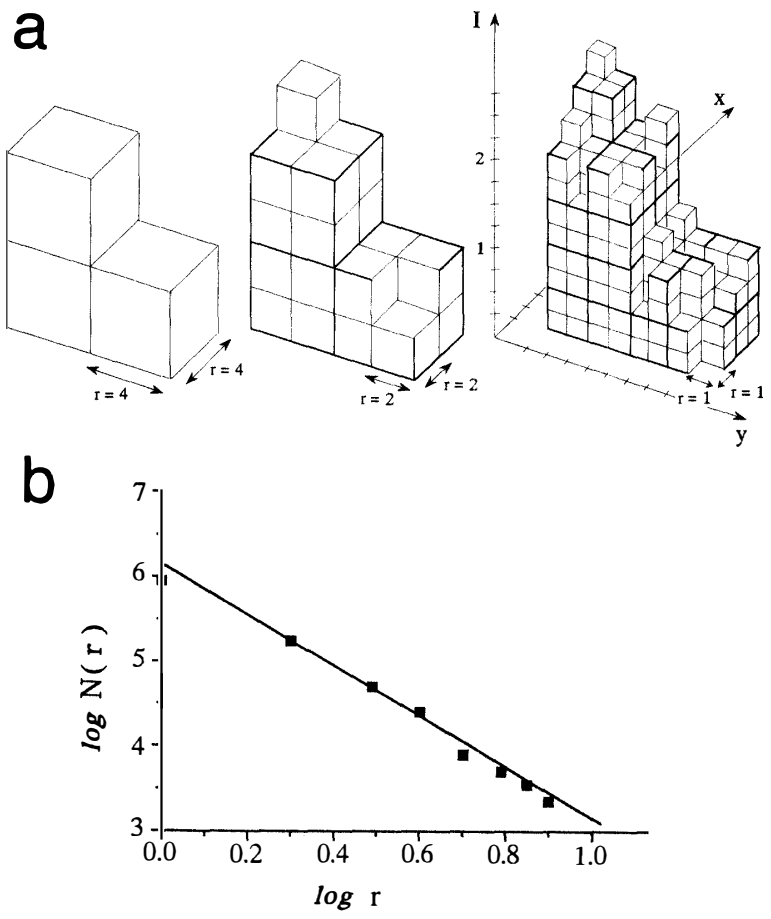

Fig. 2. (a) Image intensity surface covered with cubes. If a cube of edge r is scaled down to both the x axis and y axis, then the roughness of the gray level surface I(x, y) is proportionally increased. (b) A plot of log (edge length) versus log (total number of cubes) data.

sion on a real surface. Thus, a real surface will be fractal over some range of scales, rather than overall scales. Local fractal dimension is expressed using these limited ranges of scale (KANEKO, 1988). In this paper, local fractal dimension is calculated using continuous three edges r.

3.4. Texture

Texture is usually defined as some local property of an image, *i.e.* a measure of the relationship between the pixels in a neighborhood. There are many approaches to describe texture characteristics. One approach to texture feature extraction is based on the gray level co-occurrence matrix $P(i, j)$ (HARALICK *et al.*, 1973). This matrix denotes the probabilities of transition from one gray level to another between neighboring pixels in an image subregion of specified size. Each element of the gray level co-occurrence matrix is a measure of the probability of occurrence of two gray scale values separated by a given distance in a given direction. Generally, four angular matrices will be computed for given pixel distances corresponding to the horizontal, vertical, and two diagonal directions of the image subregion whose gray levels are i and j, respectively. In many cases, only neighboring pixels are considered for these calculations. A total of 13 scalar texture features derived from the four angular matrices were defined by HARALICK *et al.* (1973). These features are generally measures of the location and degree of concentration of pixel count in the matrix. The following equations show the two of these features.

$$uni = \sum_{i=1}^{N}\sum_{j=1}^{N}\left\{\frac{P(i,j)}{R}\right\}^2,$$

$$cor = \frac{\sum_{i=1}^{N}\sum_{j=1}^{N}\{i\cdot j\cdot P(i,j)/R\} - \mu_x\cdot\mu_y}{\sigma_x\cdot\sigma_y},$$

where N is the number of gray levels, R is a renormalizing constant equal to the total number of pixel pairs in a subregion, and μ and σ are the mean and standard deviation of the distributions of gray scale values accumulated in the x and y directions. The *uni* is a measure of uniformity, achieving its lowest value when all elements of P are equal. The *cor* is a measure of the linear dependency of gray level obtained by correlation.

4. Classification Algorithm

4.1. Classifying process

A flow chart of the classifying process is given in Fig. 3. Representative areas of clouds, sea ice and ground were selected subjectively using infrared imagery (channel 4). Average and standard deviation of gray level of each pixel, global and local fractal dimension, and uniformity and correlation of texture features of image data were computed in each selected area. The whole area of visible imagery (channel 1) was also classified manually to obtain supervised data for estimating the classification results.

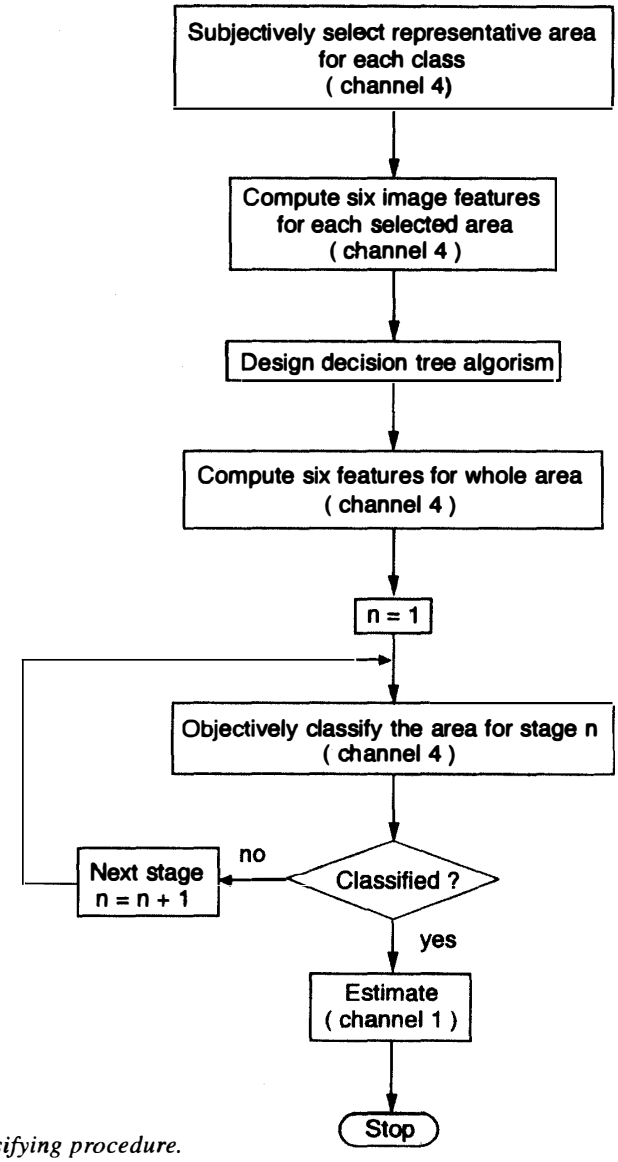

Fig. 3. Flow chart of the classifying procedure.

4.2. Training samples

In order to classify clouds, sea ice and ground, a representative area for each desired class was selected using infrared imagery. More than one training area per class was used to include the range of variability. Six features of image data of the selected areas were computed for training samples.

4.3. Decision tree classifier

The decision tree classifier is based on specified information of features in the image. This classifier is an attempt to use a series of stages or layers, with certain classes being separated at some steps of each stage in a simple manner. The thresholds of each step are determined to be separated into some classes. The separation of the remaining classes using different features is determined in a similar fashion until all the classes have been isolated. In this paper, six features of satellite data were used to design the decision tree classifier for separating three classes, cloud, sea ice and ground.

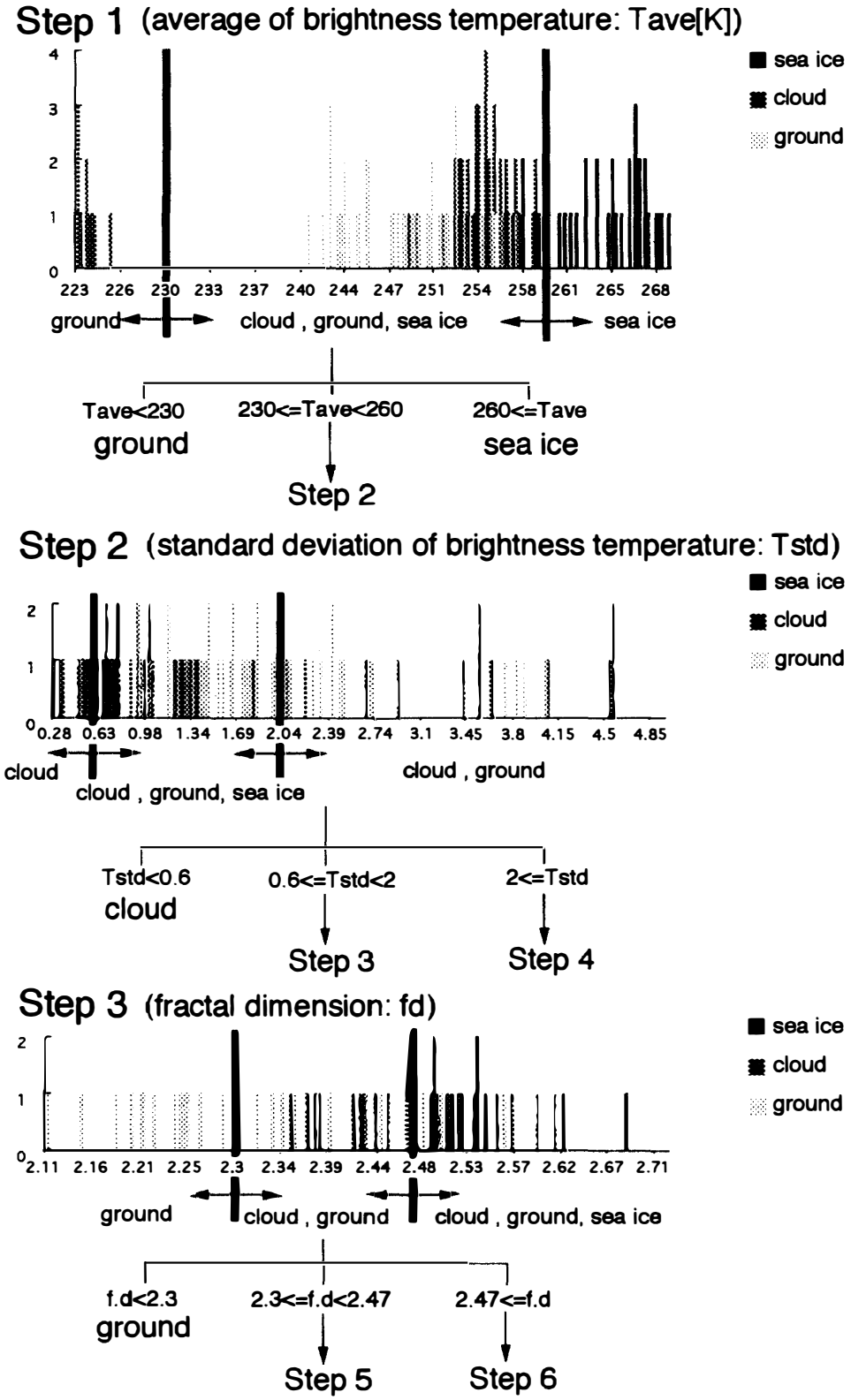

Fig. 4. Three examples of intensity histograms that can be classified by two thresholds.

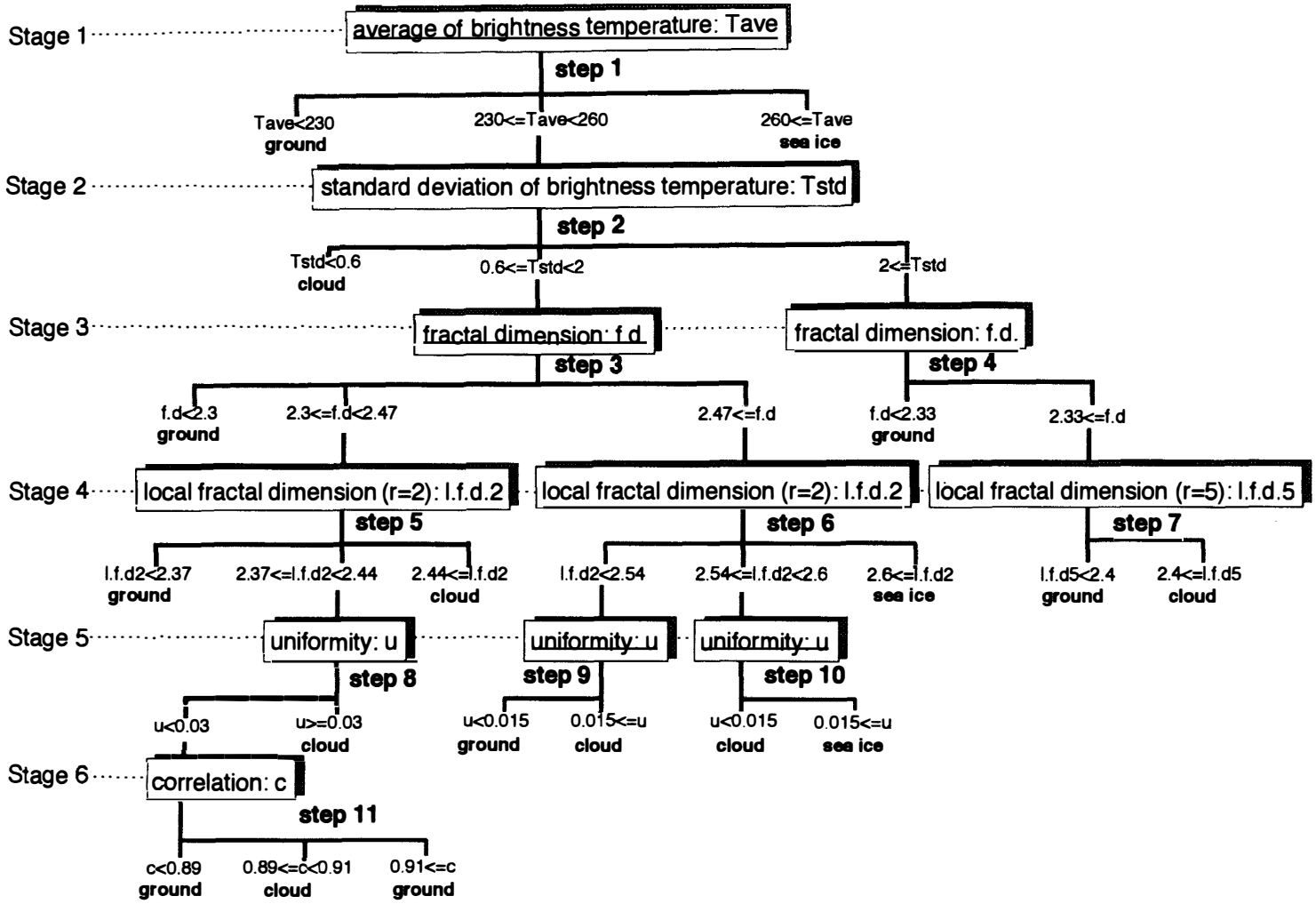

Fig. 5. Manually designed decision tree for the data in 11 steps from AVHRR image of NOAA satellite of thermal infrared channel 4. Tave: average, Std: standard deviation, f.d.: fractal dimension, l.f.d.2: local fractal dimension (r = 1, 2, 3), l.f.d.5: local fractal dimension (r = 4, 5, 6), u: uniformity, c: correlation.

5. Results and Discussion

First, six features for cloud, sea ice and ground in the satellite image were calculated using subjectively selected representative areas. These data were used to illustrate the design of a decision tree classifier. Figure 4 shows three examples of the histogram (step 1–3) and the manually-selected thresholds for three classes (cloud, sea ice and ground) with information from average and standard deviation of brightness temperature, and fractal dimension of the image. It can be seen that some part of the ground and many parts of sea ice could be separated from the others with average brightness temperature (step 1). This operation formed the first stage in the classification. Remaining regions could be separated using the standard deviation of brightness temperature (step 2). This operation therefore formed the second stage of the classification. Many parts of the ground could be separated using fractal dimension (step 3). Figure 5 shows the

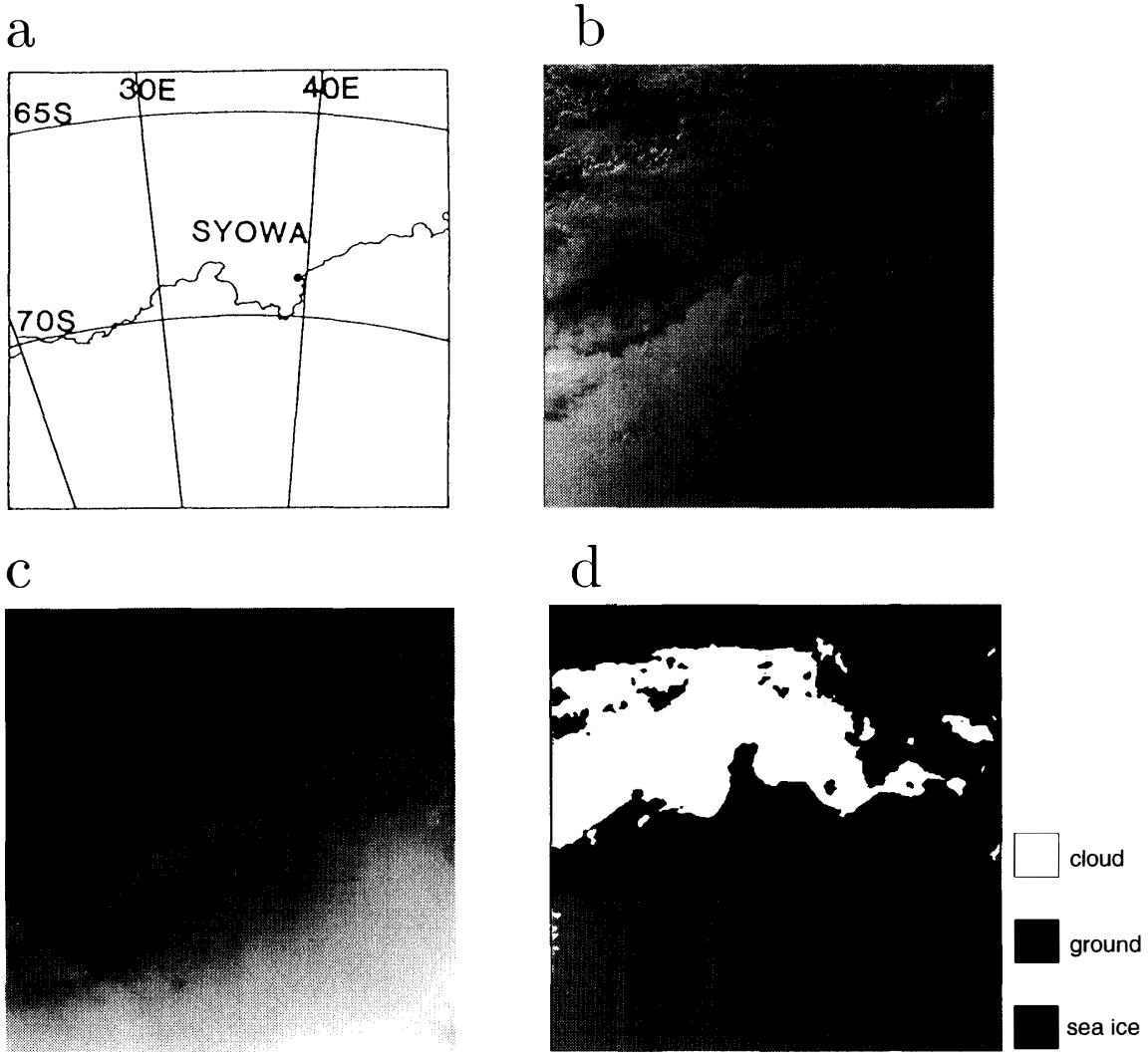

Fig. 6. Location and AVHRR image of NOAA satellite on April 8, 1989. (a) Location of the image used in analyzing. (b) Visible channel 1. (c) Thermal infrared channel 4. (d) Manually classified area for error estimation using channel 1.

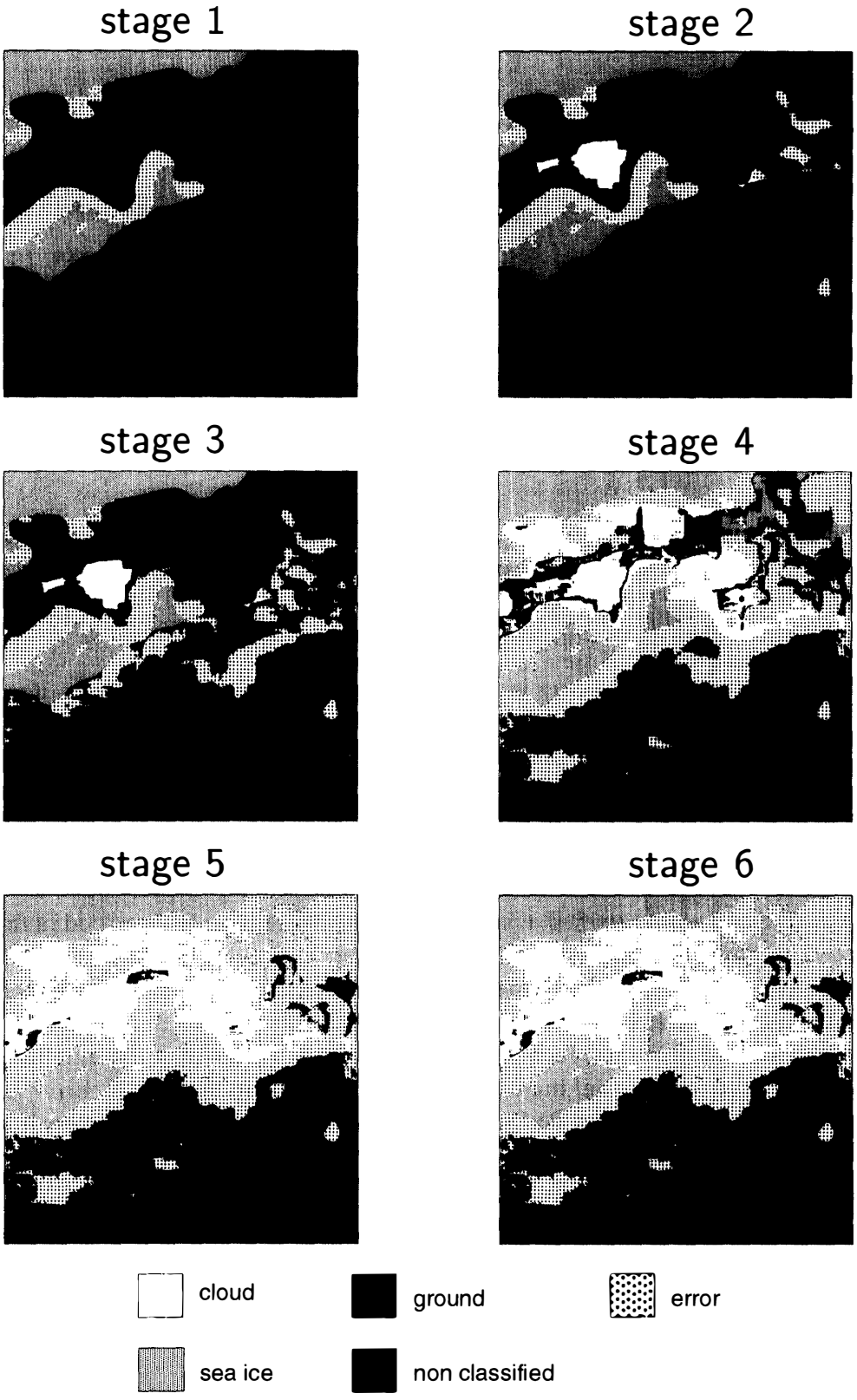

Fig. 7. Classified satellite image of thermal infrared channel 4 from stage 1 to 6.

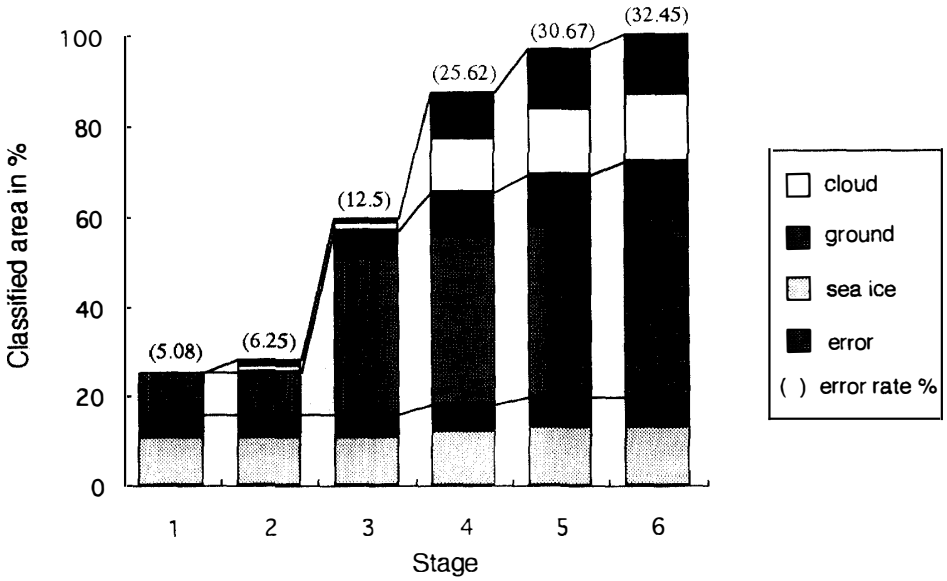

Fig. 8. The process of classification and its accuracy at each stage of the decision tree classifier. Stage 1: Average, Stage 2: Standard deviation, Stage 3: Fractal dimension, Stage 4: Local fractal dimension, Stage 5: Uniformity, Stage 6: Correlation.

final decision tree with the classes identified and features used at each stage. It is shown that each area was separated using one to seven features. Figure 6 shows the location of the image and channel 1, 4 and manually classified image of NOAA AVHRR on April 8, 1989. Figure 7 shows the classification results from stage 1 to 6 on thermal infrared channel 4 (Fig. 6c) using the decision tree classifier. Although the classified area was increased with increasing stage, the error rate was also increased. A part of ground and sea ice area were classified at stage 1, another part of ground was classified at stage 3, and a part of cloud was classified at stage 4. The other areas were classified in the same manner. Classified areas were varied in each stage.

Figure 8 shows the process of classification and its estimation of each stage. About 30% of the area was classified at stages 1, 3 and 4. Small areas were classified at stages 2, 5 and 6. The accuracy for each stage was estimated by dividing the number of correctly classified pixels by total number of classified pixels in that stage. Error rate was increased with increasing classified area. Classified areas and error rates were increased with increasing number of stages. We can say that the number of stages is decided according to the purpose.

Though sea ice and ground were largely separated from a few features, more than three features were necessary to separate clouds. These results indicate that the images contain more than one type of cloud (DESBOIS *et al.*, 1982; EBERT, 1987).

6. Conclusion

A method to segment an Antarctic satellite image using a single infrared channel of AVHRR is proposed. Average and standard deviation of gray level of each pixel, and fractal dimension and textural features of the image data, are used to determine the deci-

sion tree of classification. Among these features, average is useful for extraction of the ground, and fractal dimension is useful for extraction of the ground and cloud.

The decision tree classifier is effective in the case in which supervised data are obtained. It is a very flexible approach to separate different classes. One of the advantages of this approach is to easily add another feature for increasing classified area. Another decision tree may also be designed, because the decision tree is data-dependent. In general, simpler design is more efficient.

Acknowledgments

The authors thank N. TOKUNAGA for development of software. This work was supported partly by the Japanese Ministry of Education, Science, Sports and Culture Grants-in-Aid for Scientific Research (08650482).

References

COAKLEY, J.A. and BRETHERTON, F.P. (1982): Cloud cover from high-resolution scanner data: Detecting and allowing for partially filled fields of view. J. Geophys. Res., **87**, 4917–4932.

DESBOIS, M., SEZE, G. and SZEJWACH, G. (1982): Automatic classification of clouds on METEOSAT imagery: Application to high-level clouds. J. Appl. Meteorol., **21**, 401–412.

EBERT, E. (1987): A pattern recognition technique for distinguishing surface and cloud types in the polar regions. J. Climate Appl. Meteorol., **26**, 1412–1427.

GORDON, A.L. and TAYLOR, H.W. (1975): Seasonal change of Antarctic sea ice cover. Science, **187**, 346–347.

HARALICK, R.M., SHANMUGAM, K. and DINSTEIN, I. (1973): Textural features for image classification. IEEE Trans. Syst. Man. Cybern., **3**, 610–621.

KANEKO, H. (1988): Fractal matrix model and its application to texture analysis. Trans. IEICE, E71, **12**, 1221–1228.

MANDELBROT, B.B., PASSOJA, D.E. and PAULLAY, A.J. (1984): Fractal character of fracture surfaces of metals. Nature, **308**, 721.

MAYKUT, G. and UNTERSTEINER, N. (1971): Some results from a time-dependent thermodynamic model of sea ice. J. Geophys. Res., **76**, 1550–1575.

ROBOCK, A. (1983): Ice and snow feedbacks and the latitudinal and seasonal distribution of climate sensitivity. J. Atmos. Sci., **40**, 986–997.

SALTZMAN, B. and MORITZ, R.E. (1980): A time-dependent climate feedback system involving sea-ice extent, ocean temperature, and CO_2. Tellus, **32**, 93–118.

YAMANOUCHI, T. and KAWAGUCHI, S. (1992): Cloud distribution in the Antarctic from AVHRR data and radiation measurements at the surface. Int. J. Remote Sensing, **13**, 111–127.

YAMANOUCHI, T., KANZAWA, H., ARIYOSHI, H. and EJIRI, M. (1991) : Report on the first MOS-1 data received at Syowa Station, Antarctica. Proc. NIPR Symp. Polar Meteorol. Glaciol., **4**, 22–30.

(Received January 8, 1996; Revised manuscript accepted June 26, 1996)